BIMORPH PMUT WITH DUAL ELECTRODES

Sina Akhbari[1], Firas Sammoura[1,2], Chen Yang[1], Maitha Mahmoud[2], Nawal Aqab[2], and Liwei Lin[1]
[1]Department of Mechanical Engineering, University of California at Berkeley, Berkeley, CA, USA
[2]Department of Electrical Engineering and Computer Science, Masdar Institute of Science and Technology, Abu Dhabi, UAE

ABSTRACT

The concept of "bimorph" piezoelectric micromachined ultrasonic transducers (pMUTs) has been demonstrated by utilizing a two active AlN layers structure constructed in a CMOS-compatible process. The prototype device has two 0.95µm-thick AlN layers sandwiched by three 0.15µm-thick Mo electrodes. In a prototype, both an inner circular and an outer annular electrode are designed on a 230 µm in radius, circular-shape diaphragm. When actuated with the inner electrode of 160µm in radius, the pMUT has a resonant frequency of 198.8 kHz and central displacement of 407.4 nm/V. Under the differential drive scheme using the dual-electrodes for large acoustic outputs at a low frequency, the measured central displacement is 13.0 nm/V, which is about 400% higher than that of a unimorph AlN-pMUT under similar actuation conditions. As such, the dual-electrode bimorph pMUT presents the improved operation as compared with the state-of-the-art flat pMUT design to achieve enhanced acoustic outputs.

INTRODUCTION

Conventional ultrasound transducers are based on PZT as the piezoelectric material and operated in the thickness mode for various types of applications, including medical ultrasonography [1]. The operation resonant frequency is determined by the thickness of the PZT layer and tight process control is required to meet the targeted frequency [2]. Considering the fabrication limitations, few products involving 2D ultrasound transducer arrays are in the market. The large transducer dimensions prohibit the applications of ultrasound transducers in devices such as cell phones. In addition, piezo-ceramics inherently have high acoustic impedance, which is difficult to match with liquid or air media [3]. Nevertheless, thickness-mode PZT sensors are the current choices for applications such as distance sensors, burglar alarms, medical imaging, and nondestructive tests.

Ultrasound transducers with small form factor, linear response, low voltage, and high acoustic pressure are desirable for next generation hand-held devices. In the past twenty years, micromachined ultrasonic transducers (MUTs) have emerged as the key candidates to replace conventional ultrasound transducers with good features in acoustic matching, large bandwidth, miniaturization, and low-cost by batch fabrication [4]. Plate flexural mode operations actuated either capacitively (cMUTs [5]) or piezoelectrically (pMUTs [6]) have been developed by many researchers. MEMS fabrication technologies can be utilized and the mechanical impedance of micromachined ultrasonic transducers can be closely matched to that of the imaging medium, resulting in improved bandwidth and system efficiency. However, cMUTs require high DC voltage and small gap with known drawbacks in dielectric charging and non-linear plate deflection with applied bias [7]. On the other hand, pMUTs operate under low voltage bias with possible large diaphragm deformations for high acoustic pressure [8], while low electromechanical coupling has been a key drawback [9]. Therefore, there are various efforts to improve the electromechanical coupling of PMUTs by structural designs [10].

In order to improve the electromechanical coupling and output acoustic pressure per unit input voltage of pMUTs, designs such as the "dome-shape" piezoelectric actuators have been proposed to convert in-plane strain to flexural deflection [11]. In our previous work, PMUTs with multiple electrodes have shown enhanced effective electromechanical coupling factors, about 211% larger than that of the state-of-the-art, single electrode design [12]. A two-port pMUT using aluminum nitride (AlN) as the piezoelectric material and driven differentially with inner and outer electrodes has been validated to double the electromechanical coupling efficiency as compared with a conventional pMUT structure with 100% higher acoustic output per unit input voltage, and 485% larger suppression in magnitude of second harmonic mode [13].

This work extends the previous theoretical work on the "bimorph" pMUTs [14] using dual electrode designs with several accomplishments: (1) demonstration of a CMOS-compatible process with AlN as the piezoelectric layers; and (2) experimentally measured 400% higher output deformation as compared with the conventional unimorph pMUT by applying a differential drive scheme using the two active piezoelectric layers.

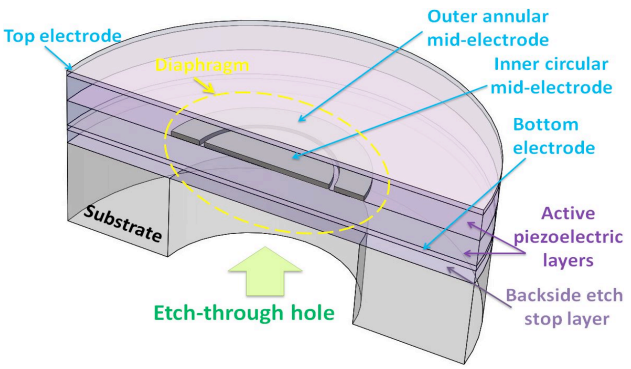

Figure 1: 3D schematic drawing showing the cross-sectional view of a bimorph pMUT with two active AlN layers and the dual electrode configuration: inner circular shape and outer annular shape electrodes.

CONCEPT

Figure 1 is a 3D schematic diagram illustrating the cross-sectional view of the bimorph pMUT design with dual-electrodes. The bimorph pMUT consists of two active piezoelectric layers, sandwiched between top, bottom, and middle electrodes.

A backside etch-through hole forms the circular diaphragm and defines its diameter. The two middle

electrodes are separated via a small gap as an inner circular-shape and outer annular-shape electrodes, which are electrically isolated and can be differentially actuated with two voltage sources of the same amplitude and opposite polarity.

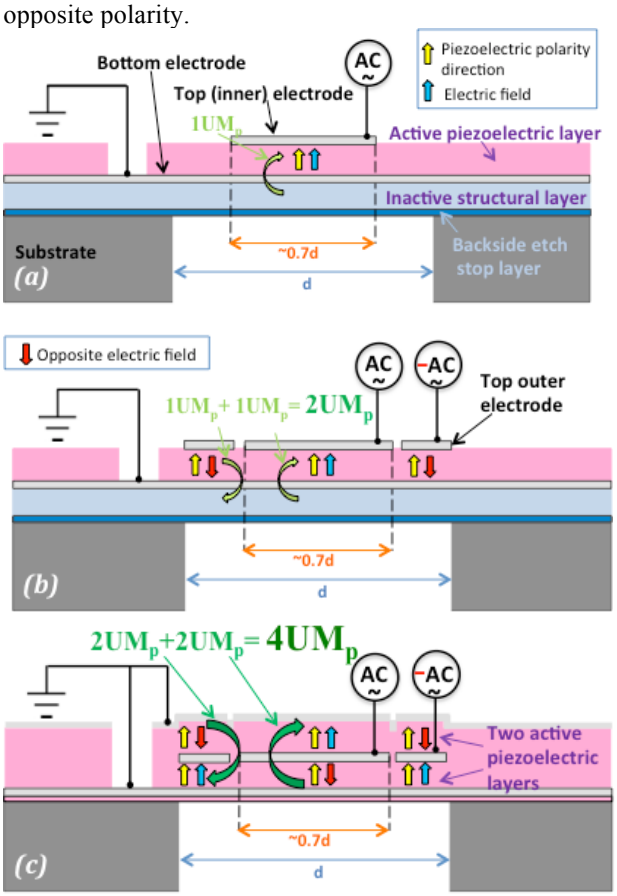

Figure 2: Cross-sectional views of (a) the conventional unimorph pMUT with one active layer; (b) the two-port unimorph pMUT with inner and outer electrodes driven differentially; and (c) the bimorph pMUT with dual electrodes to be driven differentially. It is expected to have 4X larger theoretical bending moment.

Figure 2a illustrates a conventional unimorph pMUT with a single active piezoelectric layer, a structural layer, and a top circular electrode [6]. Under an electric field between the top and bottom electrodes, an in-plane electromechanical strain is induced by the piezoelectric d_{31} effect. The strain profile generates a $1UM_p$ bending moment (UM_p is defined as an arbitrary unit of bending moment per unit input voltage) on the diaphragm and makes it move out-of-plane, i.e. in a flexural mode. A dual-electrode unimorph pMUT [13] with an inner circular and outer annular electrode is shown in Figure 2b. When driven differentially with voltage sources of the same magnitude and opposite polarity, the inner (outer) portion of the diaphragm will be in contraction while the outer (inner) portion will be in expansion to generate a $2UM_p$ bending moment. In these single active-layer devices, the electromechanical energy transformation comes from the single piezoelectric layer and some of the energy is used to mechanically deform the inactive structural layer.

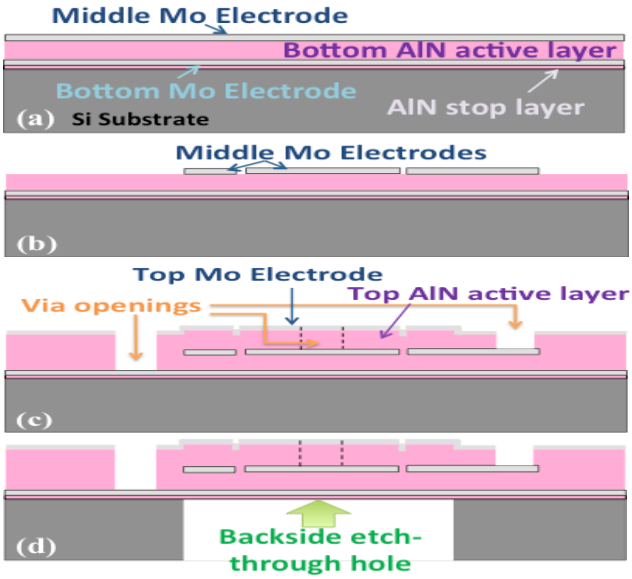

Figure 3: Process flow of the dual electrode bimorph pMUT: (a) depositions of the stop AlN layer, bottom Mo electrode, bottom AlN layer, and middle Mo electrode; (b) patterning and etching of the middle electrode; (c) depositions of the top AlN layer and top Mo electrode; opening of contacts to middle and bottom electrodes; (d) backside DRIE to release the diaphragm.

In contrast to the conventional unimorph pMUT structure and inspired by well-known cantilever-type piezoelectric bimorph structures [15], the bimorph pMUT with two active layers is shown in Figure 2c with the same polarity and separated by a patterned middle/common electrode. The top and bottom electrodes are connected to ground and the middle inner and outer electrodes are driven with AC voltages with equal magnitude but opposite phase. As such, in addition to the 2x displacement produced by the differential dual electrode similar to the case in Figure 2b, the two active layers provide another 2x larger volumetric displacement as compared with the single-layer structure. In other words, each layer generates $2UM_p$ on the diaphragm while operating in the differential mode and a total of $4UM_p$ will be imposed on the diaphragm. As such, 4x higher responses are expected by replacing the bottom structural layer by another active layer and adding the dual electrode design.

FABRICATION

Process Flow

Figure 3 shows the CMOS-compatible process flow chart for the dual-electrode bimorph pMUT, starting with: (a) sputter deposition of 200 nm-thick AlN stop layer, 150 nm-thick Mo bottom electrode, first 0.95 µm-thick AlN active layer, and 150 nm-thick middle Mo electrode; (b) patterning middle electrodes by plasma etching using SF_6; (c) sputter deposition of the second 0.95 µm-thick AlN layer and 150 nm-thick top Mo electrode. The via openings to both the middle and bottom electrodes are subsequently formed using Fluorine-based plasma to etch Mo. Chlorine-based plasma is used to etch AlN, in combination with a final wet etching step with MF-319 to clear the remaining AlN and ensure minimal damage and

maximum selectivity to the Mo electrodes; and finally (d) backside DRIE to release the diaphragm.

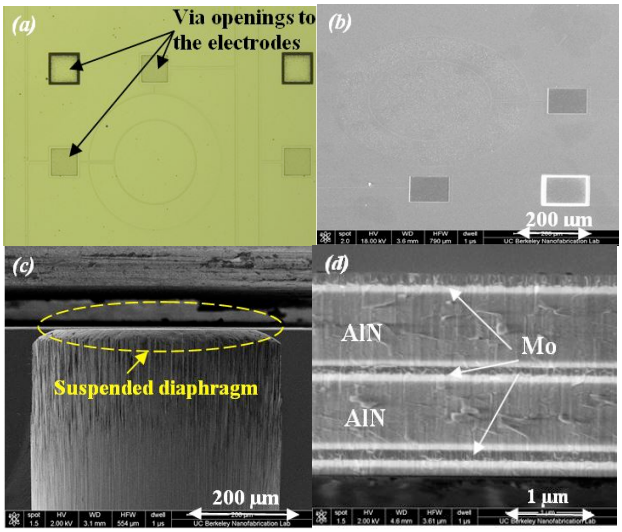

Figure 4: (a) optical top view image and (b) tilted view SEM micrograph of a dual electrode bimorph pMUT; (c) SEM image of a cleaved device showing the cross-sectional view; (d) close-up view of the diaphragm in Fig. 4c showing good crystal alignment of both AlN layers.

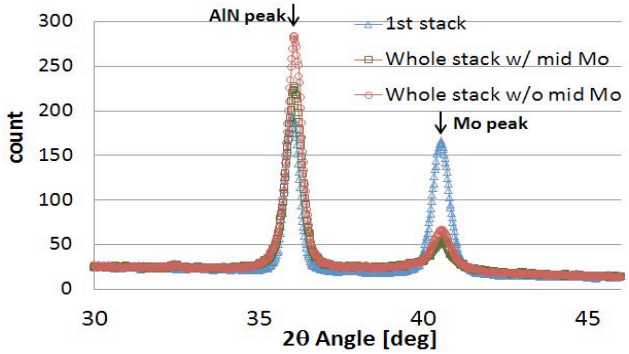

Figure 5: XRD 2θ scan of first AlN layer stack and the whole AlN stack with and without middle electrode.

Fabrication Results

Figures 4a and 4b show the respective optical and SEM top view images of a fabricated bimorph pMUT prototype with dual electrode configuration. Imprints on the top electrodes are apparent on figures, which are related to the step height variations by underlying middle electrodes. Figure 4c shows the cross-sectional SEM micrograph of a cleaved device illustrating the clamped diaphragm. Figure 4d is a close-up view of the diaphragm highlighting its layer composition, and revealing that the suspended AlN diaphragm stack has good crystal alignment in both active AlN layers.

The crystalline quality of the two active AlN layers has been further investigated using XRD (X-Ray Diffractometer), with special focus on the second AlN layer sputtered on top of the patterned middle Mo electrode as the structure has been exposed to the external environment before the deposition of the second AlN active layer. Good crystal orientation of both AlN active layers is critical for the bimorph pMUT. Figure 5 shows the XRD 2θ scans for the first sputtered single-AlN layer, and the total stack with both AlN layers. The XRD data for the total stack are collected at two different locations, the first of which is where the middle Mo electrode is sandwiched between the AlN layers, and the second of which is where the middle Mo electrode is etched away and the two AlN layers are in direct contact. Good crystallinity data of the first AlN layer and the whole stack are observed in Figure 5 at the two different scan locations. Although the XRD measurements do not reveal explicit information about the quality of the second sputtered layer, the crystalline information of the latter can be projected by comparing the collected data of the first AlN layer to the whole stack. It is observed from Figure 5 that the whole stack has a sharper peek, higher amplitude, and slightly narrower FWHM in the (002) crystalline direction than that of the first AlN layer, which indicates that the latter must be as well oriented as the first layer. The FWHM of AlN was measured to be about 1.7° from the Rocking Curve.

RESULTS AND DISCUSSIONS

Figure 6 compares the measured, theoretically derived, and simulated low frequency center displacements of a bimorph pMUT under different driving inputs by (a) inner electrode; (b) outer electrode; (c) out-of-phase drive (differential); and (d) in-phase actuation. In all driving methods, both top and bottom electrodes are grounded while inner and/or outer middle electrodes are actuated.

The dynamic responses are experimentally measured for a pMUT prototype #1 with the aforementioned stack compositions and thicknesses with inner circular electrode radius of 160 µm, and outer annular electrode radius of 230 µm using a laser Doppler vibrometer (LDV). Under the drive of the inner electrode, the DC displacement is theoretically predicted as 7.49 nm/V and experimentally measured as 7.26 nm/V. Under the outer electrode drive, the DC displacement is theoretically predicted as 7.27 nm/V and experimentally measured as 5.75 nm/V. Theoretically, the inner and outer drive should realize similar DC displacement per unit input voltage if the electrode areas are the same (the inner circular electrode radius is 70% of the pMUT diaphragm radius). The discrepancy in the measured values is attributed to the backside over etch which results in larger diaphragm than the original design. Under the differential drive operation, the measured DC displacement is 13.01 nm/V, only 11.9% lower than the theoretically predicted value of 14.76 nm/V. The differential drive mode produced roughly 2x larger displacement per unit input voltage compared with the result from single electrode actuation. Under the in-phase actuation, the DC displacement has a negligible value of 0.11 nm/V, validating the theoretical expectations and the need of middle electrodes [8].

Figure 7 compares the simulated and measured frequency responses of two pMUT prototypes. When the radius of the pMUT is reduced to 170 µm (prototype #2), a 452nm/V center displacement is measured under resonance at 344kHz. On the other hand, the measured center displacement is 407.4 nm/V under resonance at 198.9 kHz for prototype #1. This is 51% lower than the simulated value in air medium of 841.7 nm/V but is still ~4X larger than the reported results of prior unimorph flat

AlN pMUTs with similar dimensions and frequency [13]. The reduced experimental performance is related to the high residual stress (60 MPa tensile), which increases material damping. It is noted that the residual stress effect is more prominent for pMUTs with larger diaphragms.

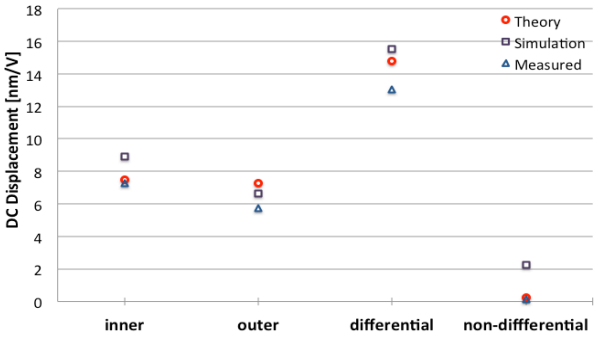

Figure 6: Measured, theoretical, and simulated low frequency displacements of a bimorph pMUT (measured resonant frequency at 206 kHz) using (1) inner electrode, (2) outer electrode, (3) differential drive, and (4) non-differential (in phase) actuation.

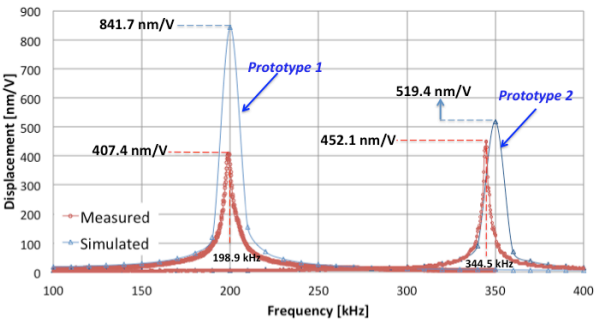

Figure 7: Measured and simulated results of two bimorph pMUTs actuated by the inner electrode with 230 and 170μm in radii and resonant frequencies of 198.9 and 344.5 kHz, respectively.

Table 1: Resonant displacement and resonant frequency of unimorph and bimorph pMUTs.

	Resonant Disp. [nm/V]	Center Freq. [kHz]
Unimorph w/annular electrode [13]	86	291
Unimorph w/ central electrode [13]	104	291
Unimorph w/ two port diff drive [13]	188	291
Bimorph (this work)	**452**	**345**

Table 1 compares the performances of previously reported unimorph pMUTs [13] with the same frequency ranges and bimorph pMUT prototypes. The table reveals that the bimorph pMUT with dual electrodes has superior performance because it has higher displacements per input voltage at higher resonant frequencies. The generated acoustic pressure is proportional to the combination of operation frequency and volumetric displacement. Thus, bimorph pMUTs are expected to generate higher pressure at higher frequency for high acoustic power transmission.

ACKNOWLEDGEMENTS

The authors would like to thank Jeffery Clarkson, Ryan Rivers, and Jay Morford from the UC Berkeley Marvell nanofabrication laboratory and Dr. Amir Heidari and Hadi Najar from the Mechanical and Aerospace Engineering Department of UC Davis for their valuable helps. This project is funded in part by GlobalFoundries Singapore Pte. Ltd. under Abu Dhabi-Singapore Twin Lab between the Institute of Microelectronics (IME) and Masdar Institute of Science and Technology, Abu Dhabi, UAE.

REFERENCES

[1] A. J. Tajik *et al.*, "Two-dimensional real-time ultrasonic imaging of the heart and great vessels. Technique, image orientation, structure identification, and validation," *Mayo Clin. Proc.*, vol. 53, no. 5, pp. 271–303, 1978

[2] G. S. Kino, Acoustic Waves: Device, Imaging, and Analog Signal Processing. Upper Saddle River, NJ: Prentice Hall, 1987.

[3] T. Ikeda, Fundamentals of Piezoelectricity, Oxford University Press, 1990.

[4] B. Khuri-Yakub, "Next-gen ultrasound," *IEEE Spectr.*, vol. 46, no. 5, pp. 44–54, May 2009.

[5] B. T. Khuri-Yakub and O. Oralkan, "Capacitive micromachined ultrasonic transducers for medical imaging and therapy," *J. Micromech. Microeng.*, vol. 21, art. no. 54004, May 2011.

[6] S. Shelton *et al.*, "CMOS-compatible AlN piezoelectric micromachined ultrasonic transducers," *in Proc. 2009 IEEE Int. Ultrason. Symp. (IUS)*, pp. 402-405, Rome, Italy, September 20-23, 2009.

[7] A. S. Ergun, G. G. Yaralioglu, and B. T. Khuri-Yakub, "Capacitive micromachined ultrasonic transducers: Theory and technology," *J. Aerosp. Eng.*, vol. 16, no. 2, pp. 76–84, 2003.

[8] K. Smyth *et al.*, "Analytic solution for N-electrode actuated piezoelectric disk with application to piezoelectric micromachnined ultrasonic transducers," *IEEE Trans. Ultrason. Ferroelectr. Freq. Control*, vol. 60, no. 8, pp. 1756–1767, Aug. 2013.

[9] P. Muralt *et al.*, "Piezoelectric micromachined ultrasonic transducers based on PZT thin films," IEEE Trans. Ultrason. Ferroelectr. Freq. Control, vol. 52, no. 12, pp. 2276–2288, Dec. 2005.

[10] F. Sammoura, K. Smyth, and S. G. Kim, "Optimizing the electrode size of circular bimorph plates with different boundary conditions for maximum deflection of piezoelectric micromachined ultrasonic transducers," *Ultrasonics*, vol. 53, pp. 328–334, Feb. 2013.

[11] S. Akhbari *et al., "Highly Responsive Curved Aluminum Nitride PMUT," in Proc. 27th IEEE Micro Electro Mechanical Syst. Conf.*, pp. 124-127, San Francisco, CA, January 26-30, 2014.

[12] F. Sammoura, S. Akhbari, N. Aqab, M. Mahmoud, and L. Lin, "Multiple Electrode Piezoelectric Micromachined Ultrasonic Transducers," *in Proc. 2014 IEEE Int. Ultrason. Symp. (IUS)*, pp. 305-308, Chicago, IL, USA, September 3-6, 2014.

[13] F. Sammoura *et al.,* "A Two-Port Piezoelectric Micromachined Ultrasonic Transducer," *in Proc. 2014 Joint IEEE ISAF/IWATMD/PFM,* pp. 1-4, State College, PA, May 12-16, 2014.

[14] F. Sammoura *et al.*, "Theoretical Modeling and Equivalent Electric Circuit of a Bimorph Piezoelectric Micromachined Ultrasonic Transducer," *IEEE Trans. Ultrason. Ferroelectr. Freq. Control*, Vol. 59, No. 5, May 2012.

[15] A. Erturk and D. J. Inman, "An experimentally validated bimorph cantilever model for piezoelectric energy harvesting from base excitations," *Smart Mater. Struct.*, vol. 18 (2009) 025009.

CONTACT

*S. Akhbari, tel: +1-510-9267150; sina.akhbari@berkeley.edu